Contribution from the Biophysics Division,
Faculty of Pharmaceutical Sciences, Teikyo University, Sagamiko, Kanagawa 199-01, Japan

EPR Studies of Hydrogen Bonding in Ferric Porphyrin Complexes. Low-Spin Dimethoxo(tetraphenylporphinato)ferrate(III) in Dimethyl Sulfoxide-Methanol

TOMOKO OTSUKA, TOSHIE OHYA, and MITSUO SATO*

Received March 15, 1984

EPR spectroscopy has been employed to characterize the hydrogen- (H-) bonded state of the low-spin Fe(III) heme complex $Fe(TPP)(OMe)_2^-$, which is formed upon mixing of Fe(TPP)Cl with excess MeO^- in Me_2SO-MeOH. Three spectrally distinct species with different sets of g values, which are designated species I-III in increasing order of anisotropy of g values, are detected depending upon the MeOH concentration in the solvent. The three low-spin species differ from one another in degree of formation of the H bond between the iron-bound MeO^- and the solvent MeOH. The H-bond formation proceeds stepwise as the MeOH concentration increases, species I-III being regarded as starting, intermediate, and ending H-bonded states, respectively. The H-bonding interaction results in a decreased crystal field around the iron, thereby causing the tetragonal and rhombic splittings in the t_2 orbitals to decrease on going from species I to II to III. This result affords a striking contrast to the H-bonding effect previously found in the low-spin complex $Fe(TPP)(ImH)_2^+$, which is discussed in connection with the crystal field parameters obtained from g values. The possibility that the H-bonding interaction may be responsible for electronic control of autoreduction of $Fe(TPP)(OMe)_2^-$ is also discussed.

Introduction

It has been recognized in recent years that hydrogen (H) bonding involving the axial ligands in iron porphyrin complexes plays a significant role in modulating electronic and reactive properties at the central metal ion.[1] EPR spectroscopy can provide valuable information about electronic structural changes caused by the H bonding. It has been demonstrated, for example, for model low-spin heme complexes $Fe(PPIX)(ImH)_2^+$[2] and $Fe(TPP)(ImH)_2^+$[3,4] that H bonding or deprotonation of the N-H moiety of coordinated imidazole leads to an increased crystal field around the iron, thereby causing alterations in d-orbital energy level. This information affords a basis for interpreting the electronic alterations observed in hemoproteins with proximal histidyl imidazole such as cytochromes b_5[5] and c[6] and hemoglobin derivatives.[7] In addition, it is suggested that such an H-bonding interaction is largely responsible for electronic control of heme reactivity.[8]

In general, the modes of H bonding involving the coordinated ligands are conveniently divided into two types: the metal-bound ligand acts as a proton donor in the first type of H bonding, while it acts as a proton acceptor in the second type. The mode of H bonding in hemoproteins[5-9] with proximal histidyl imidazole and in low-spin bis(imidazole) complexes[2,3,10] is typical of the first type. This type of H bonding has been substantiated also in high-spin complexes $Fe(TPP)(H_2O)_2^+$[11] and $Fe(OEP)(MeOH)_2^+$.[12] By contrast, the second type of H bonding has been recognized in such model heme complexes as $Fe(p)(CN)_2^-$,[13] Fe(p)(py)(CN),[13,14] and $Fe(TPP)F_2^-$[15] (where p = PPIX, PPIXDME, TPP). However, electronic structural changes caused by the second type of H bonding seem to be poorly characterized in particular by EPR spectroscopy.

In an attempt to help our understanding of electronic control of heme reactivity in hemoproteins, we have currently started EPR studies on the H bonding involving the axial ligands of model heme complexes. In the present work, we report on the second type of H bonding found in low-spin dimethoxo(tetraphenylporphinato)ferrate(III), $Fe(TPP)(OMe)_2^-$. EPR characteristics obtained for $Fe(TPP)(OMe)_2^-$ that was formed in toluene-MeOH were described previously.[16] The g values were found to be independent of the solvent composition, which led us to conclude that a single low-spin species is present in toluene-MeOH. In contrast to this observation, however, we have found that the low-spin complex $Fe(TPP)(OMe)_2^-$, when Me_2SO-MeOH is used as solvent in place of toluene-MeOH, exists in three spectrally distinct states with different sets of g values depending upon the MeOH concentration in the solvent. The three low-spin states are interpreted as being different in degree of H-bond formation between the iron-bound MeO^- and the solvent MeOH. It will be shown that the H-bonding interaction in $Fe(TPP)(OMe)_2^-$ leads to a decreased crystal field around the iron, in marked contrast to that in $Fe(TPP)(ImH)_2^+$. The two types of H-bonding interaction modulate the electronic structure in opposite directions, which is discussed in connection with the crystal field parameters obtained from g values. This paper also reports on the autoreduction of $Fe(TPP)(OMe)_2^-$, which is controlled by the H-bonding interaction.

Experimental Section

Materials. Fe(TPP)Cl was synthesized by literature methods[17] using chlorin-free $TPPH_2$[18] and was purified by dry column chromatography on Al_2O_3 with chloroform and by recrystallization from chloroform-hexane. Fe(TPP)(OMe) was prepared as described previously.[16] Sodium methoxide (NaOMe, ca.28% in MeOH) was purchased from Wako Chemicals and used as obtained or after dilution with MeOH. The

(1) Doeff, M. M.; Sweigart, D. A. *Inorg. Chem.* **1982**, *21*, 3699. Doeff, M. M.; Sweigart, D. A.; O'Brien, P. *Ibid* **1983**, *22*, 851 and references therein.
(2) Peisach, J.; Blumberg, W. E.; Adler, A. *Ann. N.Y. Acad. Sci.* **1973**, *206*, 310.
(3) Quinn, R.; Nappa, M.; Valentine, J. S. *J. Am. Chem. Soc.* **1982**, *104*, 2588.
(4) Abbreviations: TPP, tetraphenylporphyrin dianion; OEP, octaethylporphyrin dianion; PPIX, protoporphyrin IX dianion; PPIXDME, protoporphyrin IX dimethyl ester dianion; DPIXDME, deuteroprotoporphyrin IX dimethyl ester dianion; ImH, imidazole; Im^-, imidazolate anion; py, pyridine; Pip, piperidine; Me_2SO, DMSO, dimethyl sulfoxide; DPPH, diphenylpicrylhydrazyl.
(5) Ikeda, M.; Iizuka, T.; Takao, H.; Hagihara, B. *Biochim. Biophys. Acta* **1974**, 336, 15. Bois-Poltoratsky, R.; Ehrenberg, A. *Eur. J. Biochem.* **1967**, *2*, 361. Peisach, J.; Mims, W. B. *Biochemistry* **1977**, *16*, 2795.
(6) Brautigan, D. L.; Feinberg, B. A.; Hoffman, B. M.; Margoliash, E.; Peisach, J.; Blumberg, W. E. *J. Biol. Chem.* **1977**, *252*, 574.
(7) Chevion, M.; Salhany, J. M.; Peisach, J.; Castillo, C. L.; Blumberg, W. E. *Isr. J. Chem.* **1977**, *15*, 311.
(8) Stanford, M. A.; Swartz, J. C.; Phillips, T. E.; Hoffman, B. M. *J. Am. Chem. Soc.* **1980**, *102*, 4492 and references therein.
(9) Valentine, J. S.; Sheridan, R. P.; Allen, L. C.; Kahn, P. C. *Proc. Natl. Acad. Sci. U.S.A.* **1979**, *76*, 1009. La Mar, G. N.; De Ropp, J. S.; Chacko, V. P.; Satterlee, J. D.; Erman, J. S. *Biochim. Biophys. Acta* **1982**, *708*, 317.
(10) Satterlee, J. D.; La Mar, G. N.; Frye, J. S. *J. Am. Chem. Soc.* **1976**, *98*, 7275. Walker, F. A.; Lo, M. W.; Ree, M. T. *Ibid.* **1976**, *98*, 5552. Balch, A. L.; Watkins, J. J.; Doonan, D. J. *Inorg. Chem.* **1979**, *18*, 1228.
(11) Kastner, M. E.; Scheidt, W. R.; Mashiko, T.; Reed, C. A. *J. Am. Chem. Soc.* **1978**, *100*, 666.
(12) Morishima, I.; Kitagawa, S.; Matsuki, E.; Inubushi, T. *J. Am. Chem. Soc.* **1980**, *102*, 2429.
(13) La Mar, G. N.; Del Gaudio, J.; Frye, J. S. *Biochim. Biophys. Acta* **1977**, *498*, 422. Morishima, I.; Inubushi, T. *J. Chem. Soc., Chem. Commun.* **1977**, 616.
(14) Scheidt, W. R.; Lee, Y. J.; Luangdilok, W.; Haller, K. J.; Anzai, K.; Hatano, K. *Inorg. Chem.* **1983**, *22*, 1516.
(15) Scheidt, W. R.; Lee, Y. J.; Tamai, S.; Hatano, K. *J. Am. Chem. Soc.* **1983**, *105*, 778.
(16) Otsuka, T.; Ohya, T.; Sato, M. *Inorg. Chem.* **1984**, *23*, 1777.
(17) Adler, A. D.; Longo, F. R.; Kampas, F.; Kim, J. *J. Inorg. Nucl. Chem.* **1970**, *32*, 2443.
(18) Adler, A. D.; Longo, F. R.; Finarelli, J. D.; Goldmacher, J.; Assour, J.; Korsakoff, L. *J. Org. Chem.* **1967**, *32*, 476. Barnett, G. H.; Hudson, M. F.; Smith, K. M. *Tetrahedron Lett.* **1973**, 2887.

0020-1669/85/1324-0776$01.50/0

Table I. Visible and EPR Spectral Data for the Complex Species Formed upon Mixing Fe(TPP)Cl with MeO^- in Me_2SO–MeOH

complex	conditions	visible (at 298 K) λ_{max}, nm (ϵ, mM^{-1} cm^{-1})	EPR (at 15 K) g_x	g_y	g_z	spin state
$Fe(TPP)(Me_2SO)_2^+$	Me_2SO or Me_2SO–MeOH (75:25 v/v)	415 (110), 497 (11), 530 (14), 687 (3.3)	6.04	6.04	2.00	
$Fe(TPP)(OMe)(Me_2SO)$	Me_2SO or Me_2SO–MeOH (99:1 v/v), $+MeO^-$	422 (110), 575 (9.0), 615 (6.0)	~6[a]	~6[a]	~2	high-spin ($S = 5/2$)
Fe(TPP)(OMe)(MeOH)	Me_2SO–MeOH (75:25 v/v), $+MeO^-$	420 (110), 580 (8.2), 625 (5.3)	5.55	6.40	1.99	
$Fe(TPP)(OMe)_2^-$ [b]	Me_2SO–MeOH (99:1 v/v), $+MeO^-$ (excess)	438 (140), 550 (9.9), 597 (8.8), 638 (7.5)	1.942[d] 1.928[e]	2.134[d] 2.151[e]	2.394[d] 2.442[e]	low-spin ($S = 1/2$)
	Me_2SO–MeOH (97:3 v/v), $+MeO^-$ (excess)	436 (130), 550 (8.3), 595 (8.0), 640 (6.6)	1.914[f]	2.165[f]	2.494[f]	
ferrous species[c]	Me_2SO–MeOH (97:3 v/v), $+MeO^-$ (excess) under N_2	417, 450, 535, 580, 622	not observed			unknown

[a] Line width broadening presumably caused by aggregation indicates small rhombic splitting ($g_x \neq g_y$). [b] Two spectrally distinct species were detected by visible absorptions, while three distinct species were found by EPR absorptions. The latter three species are designated species I–III, in increasing order of anisotropy of g values. The conditions for observation of species I–III are given in the text. [c] Probably mixtures of two reduced species $Fe(TPP)(OMe)_2^{2-}$ and $Fe(TPP)(OMe)(MeOH)^-$. [d] Species I. [e] Species II. [f] Species III.

accurate concentration of MeO^- in MeOH was determined by titration with hydrochloric acid with phenolphthalein as indicator. Tetraethylammonium fluoride ($Et_4NF{\cdot}2H_2O$) was obtained from Tokyo Kasei Chemicals and was dried under high vacuum at 80 °C prior to use. The crown ether (18-crown-6) complex of sodium dithionite was prepared in Me_2SO following published methods.[19] Me_2SO was purified by distillation over calcium hydride under reduced pressure and stored over 4A molecular sieves. MeOH was of spectrograde quality (Dojin Chemicals) and was used without further purification.

Procedures. Fe(TPP)Cl was dissolved in mixed-solvent Me_2SO–MeOH, yielding complex species identified as $Fe(TPP)(Me_2SO)_2^+$. Samples for EPR measurements were prepared by adding MeO^- to $Fe(TPP)(Me_2SO)_2^+$ in Me_2SO–MeOH with vigorous stirring at room temperature. The concentrations were varied systematically in the ranges $[Fe(TPP)(Me_2SO)_2^+]_0 \simeq 0.5$–1.5 mM, $[MeO^-]_0/[Fe(TPP)(Me_2SO)_2^+]_0 = 0$–100, and MeOH concentration 1–25% (v/v), where the subscript zero refers to the initial concentration. The concentration of fluoride anion was varied from $[F^-]_0 = 0$–500 mM by adding a known weight of solid tetraethylammonium fluoride. The sample solutions were transferred into quartz tubes (4.0 mm i.d.) and frozen at 77 K within a few minutes to avoid side reactions.

Samples for visible spectroscopic measurements were prepared similarly in quartz 10-mm cells. The concentrations were $[Fe(TPP)(Me_2SO)_2^+]_0 = 0.005$–0.010 mM and $[MeO^-]_0/[Fe(TPP)(Me_2SO)_2^+]_0 = 0$–1500. For experiments on autoreduction, N_2 or air was bubbled through the solutions or excess 18-crown-6 complex of sodium dithionite was added.

Measurements. EPR measurements were made at 77 K or below with a JEOL FE3AX spectrometer with 100-kHz field modulation. The magnetic field was calibrated with anNMR gaussmeter (ES-FC4, JEOL), and the microwave frequency was determined by use of a DPPH reference ($g = 2.0036$). The g values were determined at the peak (or trough) and at the middle point of the first-derivative spectrum. Temperatures below 77 K were attained with a Heli-tran variable-temperature system (LTD-3-110, Air Products Co). The spectra showed the general trend of line width broadening toward higher temperatures but with almost constant g values.

Visible spectra were measured with a Hitachi 200-10 spectrophotometer. Temperatures between 0 and 50 °C were controlled with a thermostating cell holder (Type 0510, Hitachi).

Results and Discussion

Complex Species in Me_2SO–MeOH. The high- and low-spin complex species that are formed upon mixing of Fe(TPP)Cl with MeO^- in Me_2SO–MeOH are listed in Table I together with their visible and EPR characteristics. It has been reported[20] that hexacoordinate high-spin complex $Fe(TPP)(Me_2SO)_2^+$ is formed with complete dissociation of chloro ligand when Fe(TPP)Cl is dissolved in Me_2SO. We confirmed spectroscopically the same species $Fe(TPP)(Me_2SO)_2^+$ predominantly existing in the mixed-solvent Me_2SO–MeOH of varying MeOH concentration up to 25% (v/v). The high-spin monomethoxo complexes, Fe(TPP)(OMe)(Me_2SO) and Fe(TPP)(OMe)(MeOH), were identified by comparing their visible and EPR spectra with those obtained by dissolving crystalline solid Fe(TPP)(OMe) directly in Me_2SO and Me_2SO–MeOH (75:25 v/v), respectively. These monomethoxo complexes were ascertained to be reaction intermediates (vide infra). The low-spin complex $Fe(TPP)(OMe)_2^-$ was confirmed by its characteristic EPR absorptions as described previously,[16] the spectral changes showing the processes of $Fe(TPP)(OMe)_2^-$ formation being given in the next section. The low-spin complex $Fe(TPP)(OMe)_2^-$ was liable to autoreduce in

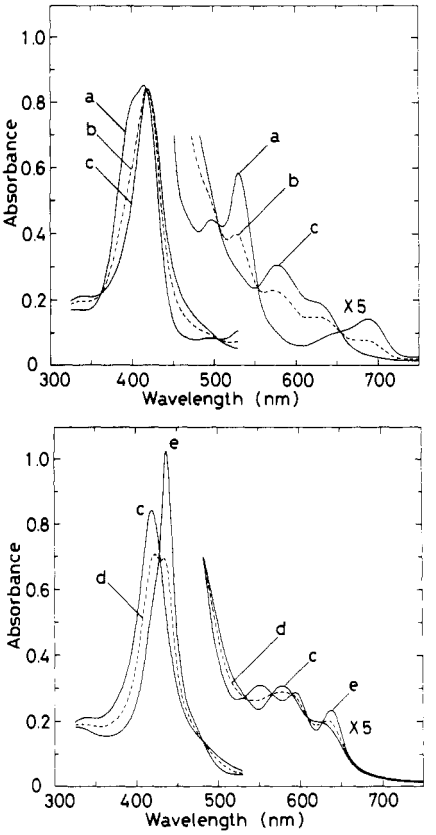

Figure 1. Visible spectral changes at 298 K for titration of $Fe(TPP)(Me_2SO)_2^+$ in Me_2SO–MeOH (97:3 v/v) with MeO^-. Conditions: $[Fe(TPP)(Me_2SO)_2^+]_0 = 0.0076$ mM; $[MeO^-]_0/[Fe(TPP)(Me_2SO)_2^+]_0 = 0$ (a), 4.5 (b), 6.8 (c), 140 (d), 1260 (e); curves a, c, and e, solid lines; curves b and d, broken lines. Two sets of isosbestic points are observed: one set is seen at 362, 417, 505, 553, and 654 nm for $[MeO^-]_0/[Fe(TPP)(Me_2SO)_2^+]_0 < 6$ (upper figure), while the other, at 427, 480, 530, 570, 590, 610, and 630 nm for $[MeO^-]_0/[Fe(TPP)(Me_2SO)_2^+]_0 = 100 \sim 1000$ (lower figure). Curves c and e are assigned to Fe(TPP)(OMe)(MeOH) and $Fe(TPP)(OMe)_2^-$, respectively.

(19) Mincey, T.; Traylor, T. G. *Bioinorg. Chem.* **1978**, *9*, 409.
(20) Brown, S. B.; Lantzke, I. R. *Biochem. J.* **1969**, *115*, 279. Mashiko, T.; Kastner, M. E.; Spartalian, K.; Scheidt, W. R.; Reed, C. A. *J. Am. Chem. soc.* **1978**, *100*, 6354. Bottomley, L. A.; Kadish, K. M. *Inorg. Chem.* **1981**, *20*, 1348.

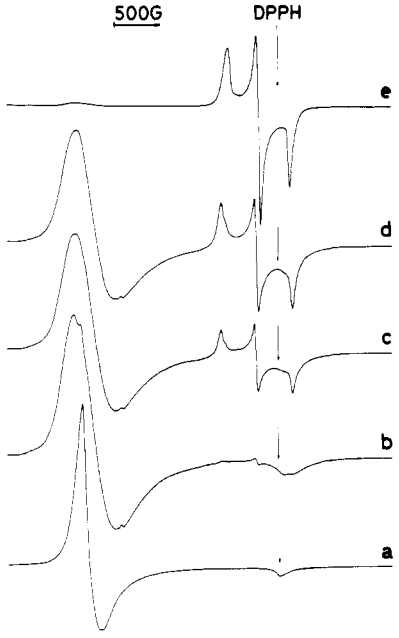

Figure 2. EPR spectra at 15 K of $Fe(TPP)(Me_2SO)_2^+$ in Me_2SO–MeOH (99:1 v/v) in the absence or presence of MeO^-. Conditions: $[Fe(TPP)(Me_2SO)_2^+]_0$ = 1.4 mM; $[MeO^-]_0/[Fe(TPP)(Me_2SO)_2^+]_0$ = 0 (a), 2 (b), 5 (c), 10 (d), 50 (e).

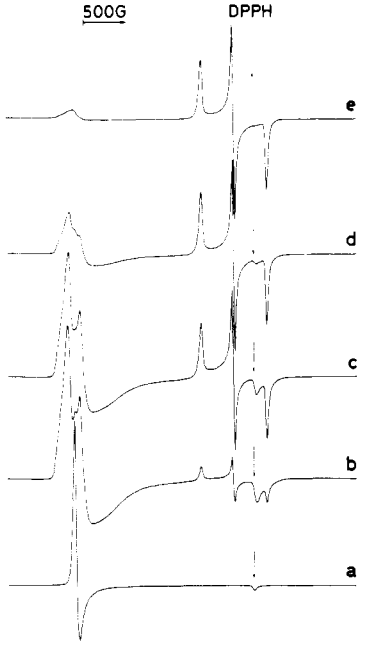

Figure 3. EPR spectra at 15 K of $Fe(TPP)(Me_2SO)_2^+$ in Me_2SO–MeOH (75:25 v/v) in the absence or presence of MeO^-. Conditions: $[Fe(TPP)(Me_2SO)_2^+]_0$ = 1.4 mM; $[MeO^-]_0/[Fe(TPP)(Me_2SO)_2^+]_0$ = 0 (a), 2 (b), 5 (c), 10 (d), 50 (e).

the absence of air, yielding Fe(II) species in unknown spin state.

Formation of $Fe(TPP)(OMe)_2^-$. Addition of excess MeO^- to $Fe(TPP)(Me_2SO)_2^+$ in Me_2SO–MeOH resulted in the formation of the low-spin complex $Fe(TPP)(OMe)_2^-$. Visible and EPR spectral changes showing the stepwise formation of $Fe(TPP)(OMe)_2^-$ are illustrated in Figures 1–3. Two sets of isosbestic points in the visible spectral changes (Figure 1) indicate that stepwise binding of MeO^- to iron takes place with much greater ease in the first-step reaction than in the second-step one. This reaction feature was confirmed in the solvent of MeOH concentrations ranging from 1 to 25% (v/v). The intermediate complex identified as $Fe(TPP)(OMe)(Me_2SO)$ was observed in the solvent of low MeOH concentrations (1–2% (v/v)), while that identified as Fe(TPP)(OMe)(MeOH), in the solvent of relatively high MeOH concentrations (3–25% (v/v)). Typical EPR spectra for

Scheme I

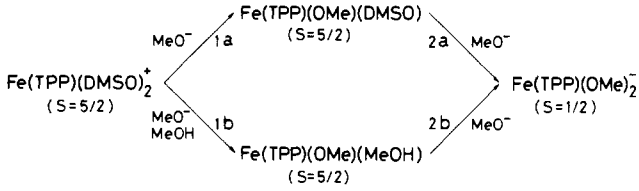

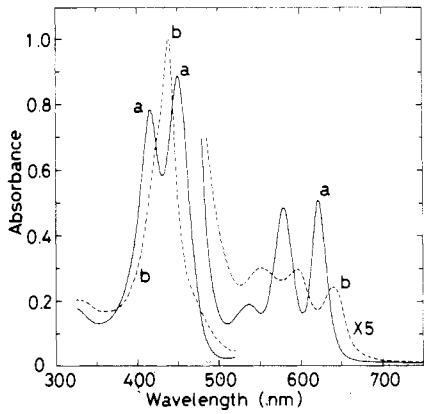

Figure 4. Visible spectrum at 298 K: (a) obtained by adding MeO^- to $Fe(TPP)(Me_2SO)_2^+$ in Me_2SO–MeOH (97:3 v/v) under N_2 (solid line); (b) obtained after bubbling air through the solution (broken line). Conditions: $[Fe(TPP)(Me_2SO)_2^+]_0$ = 0.0075 mM; $[MeO^-]_0/[Fe(TPP)(Me_2SO)_2^+]_0$ = 400.

Fe(TPP)(OMe)(Me_2SO) and Fe(TPP)(OMe)(MeOH) can be seen in Figures 2 and 3, respectively. The second-step reaction was confirmed by using Fe(TPP)(OMe) in place of Fe(TPP)Cl as starting material. It is noted that the methoxo ligand of Fe(TPP)(OMe) does not dissociate in Me_2SO and Me_2SO–MeOH in contrast to the chloro ligand of Fe(TPP)Cl. The visible spectra were temperature dependent, and the binding of MeO^- was found to be exothermic in both the first- and second-step reactions. A large difference in formation of $Fe(TPP)(OMe)_2^-$ for a given $[MeO^-]_0/[Fe(TPP)(Me_2SO)_2^+]_0$ between visible and EPR results can be explained by taking this temperature effect into consideration.[21]

On the basis of these observations, the reaction processes for $Fe(TPP)(OMe)_2^-$ formation are summarized as depicted in Scheme I. The second-step reactions (2a,b) accompany a spin state change from the high spin ($S = {}^5/_2$) of Fe(TPP)(OMe)(Me_2SO) and Fe(TPP)(OMe)(MeOH) to the low spin ($S = {}^1/_2$) of $Fe(TPP)(OMe)_2^-$. Such a spin state change is in accordance with the view[22] that MeO^- is a much stronger field ligand than neutral MeOH or Me_2SO. In one aspect, the low-spin complex $Fe(TPP)(OMe)_2^-$ may be regarded as a deprotonated form of the high-spin complex Fe(TPP)(OMe)(MeOH). If that is the case, a strongly basic medium is favorable for stabilizing $Fe(TPP)(OMe)_2^-$, and such condition is satisfied by adding a large amount of MeO^- to Me_2SO–MeOH. In another aspect, however, $Fe(TPP)(OMe)_2^-$ may be regarded as a ligand-replaced form of Fe(TPP)(OMe)(MeOH). In brief, MeO^- is considered to act as a proton acceptor or replacing ligand in reaction 2b, while it acts as a replacing ligand in reactions 1a, 1b, and 2a.

Autoreduction of $Fe(TPP)(OMe)_2^-$. It has been reported by Chang et al.[23] that, when Fe^{III}(PPIXDME)Cl is mixed with MeO^- in Me_2SO in the absence of air, Fe^{III} ion autoreduces rapidly, yielding the Fe^{II} complex of dimethoxo coordination. In accordance with this observation, the solution of $Fe(TPP)(Me_2SO)_2^+$ mixed with excess MeO^- in Me_2SO–MeOH under N_2 exhibited

(21) It is noted that $Fe(TPP)(OMe)_2^-$ is formed considerably during the process of freezing the EPR sample solution. The EPR results shown in Figure 2 should be compared with those in Figure 3 by considering a significant difference in freezing point between the two mixed solvents.
(22) Houghton, R. P. "Metal Complexes in Organic Chemistry"; Cambridge University Press: Cambridge, 1979.
(23) Chang, C. K.; Dolphin, D. *Proc. Natl. Acad. Sci. U.S.A.* **1976**, *73*, 3338.

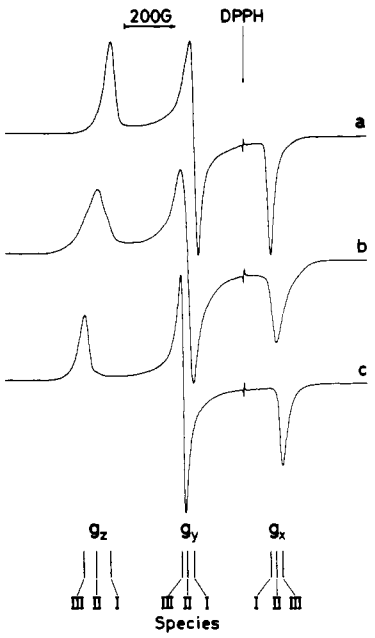

Figure 5. EPR spectra at 15 K typical of species I–III of Fe(TPP)-$(OMe)_2^-$. Conditions: $[Fe(TPP)(Me_2SO)_2^+]_0$ = 1.4 mM; $[MeO^-]_0/[Fe(TPP)(Me_2SO)_2^+]_0$ = 50. Key: (a) species I, $[F^-]_0$ = 500 mM, Me_2SO–MeOH (97:3 v/v); (b) species II, Me_2SO–MeOH (98:2 v/v); (c) species III, Me_2SO–MeOH (75:25 v/v). Peak assignments of g_x, g_y, and g_z absorptions are indicated at the bottom.

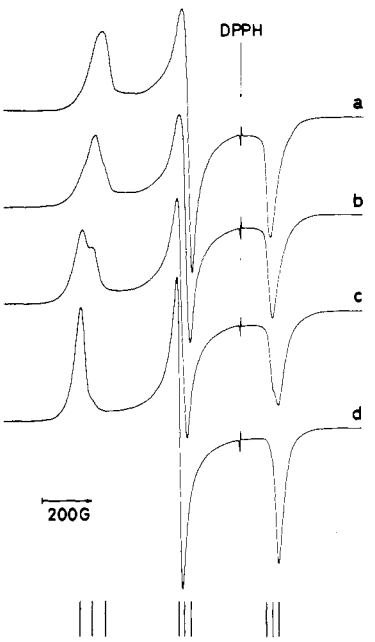

Figure 6. Effect of MeOH concentration on EPR spectra of Fe-$(TPP)(OMe)_2^-$ at 77 K. Conditions: $[Fe(TPP)(Me_2SO)_2^+]_0$ = 1.4 mM; $[MeO^-]_0/[Fe(TPP)(Me_2SO)_2^+]_0$ = 50. Key: (a) Me_2SO–MeOH (99:1 v/v); (b) Me_2SO–MeOH (98:2 v/v); (c) Me_2SO–MeOH (97:3 v/v); (d) Me_2SO–MeOH (75:25 v/v). See Figure 5 for peak assignments at the bottom.

a visible spectrum identical with that obtained by reducing Fe-$(TPP)(OMe)_2^-$ with the 18-crown-6 complex of sodium dithionite. When air was bubbled through the solution, the spectrum reverted to that characteristic of $Fe(TPP)(OMe)_2^-$, indicating that Fe^{II} species formed under N_2 were reoxidized upon air bubbling. A typical spectral change is illustrated in Figure 4.

The autoreduction of $Fe(TPP)(OMe)_2^-$ was solvent dependent, being observed in the solvent of low MeOH concentration. The reduction rate increased as the MeOH concentration was decreased: the reactive property of $Fe(TPP)(OMe)_2^-$ is greatly affected by MeOH in the solvent. The iron-bound MeO^- acts as an H-bond acceptor toward MeOH. Such an interaction would make the autoreduction of $Fe(TPP)(OMe)_2^-$ more difficult to take place. The Fe^{II} species formed in Me_2SO–MeOH were quite stable so long as air was carefully excluded. However, when the solution was exposed to air, reoxidation of the Fe^{II} species proceeded rapidly to yield $Fe(TPP)(OMe)_2^-$. This result is contrasted to the formation of oxo-bridged dimer usually encountered in the oxidation of ferrous porphyrins[24] but resembles the unusual lack of dimer formation found in the oxidation of $Fe^{II}(TPP)(CN)_2^{2-}$.[25]

It is noted in Figure 4 that the Soret band at 436 nm is replaced by the two bands at 417 and 450 nm on going from Fe(TPP)-$(OMe)_2^-$ to the Fe^{II} species. The two Soret bands of the Fe^{II} species varied in their relative absorbances depending upon the MeOH concentration, suggesting that two reduced complex species, probably $Fe^{II}(TPP)(OMe)_2^{2-}$ and $Fe^{II}(TPP)(OMe)(MeOH)^-$,[26] are present in the solution.

Incidentally, the absorption maximum at 450 nm for the Fe^{II} species has a close resemblance in the wavelength to those for cytochromes CO-P-450[27] and H-450.[28] Such large, red shifts in Soret bands have been observed also in model Fe^{II} porphyrin complexes with the anionic axial ligands RS^-, RO^-, and Im^-.[23,29] In CO-P-450, the fifth axial ligand is generally thought to be a cysteinethiolate anion. However, the axial coordination in H-450 has not yet been pursued in detail. Our contention is that anionic ligands such as RS^-, RO^-, and Im^- from amino acid residues are possible candidates for the fifth and/or sixth axial coordination of H-450.

Factors Affecting EPR Spectra of $Fe(TPP)(OMe)_2^-$. Among the complex species summarized in Table I, particularly noteworthy is the low-spin complex $Fe(TPP)(OMe)_2^-$ for which three spectrally distinct species are detected by EPR absorptions. The representative EPR spectra recorded at 15 K are compared in Figure 5. The visible spectra for $Fe(TPP)(OMe)_2^-$ varied appreciably depending upon the MeOH concentration, which is also indicative of at least two spectrally distinct species existing in the solution. All these spectrally distinct species can formally be assigned to the coordination $Fe(TPP)(OMe)_2^-$. However, they differ from one another in the state of H bonding involving the coordinated axial ligands. In what follows, the three species distinguished by EPR absorptions are designated species I–III in increasing order of anisotropy of g values.

(a) MeOH Concentration. To make clear H-bonded states of species I–III, EPR spectra of $Fe(TPP)(OMe)_2^-$ were observed in the mixed-solvent Me_2SO–MeOH of varying MeOH concentrations. Some typical spectra obtained at 77 K[30] are shown in Figure 6. Species I exists in preference to species II and III in the solution of low MeOH concentration (ca. 1% (v/v)). An increase in MeOH concentration results in the conversion of species I into II, the spectrum of species II gaining its maximum intensity at the MeOH concentration ca. 2% (v/v). As MeOH concentration is increased above 2% (v/v), species II is gradually replaced by species III, and above 5% (v/v), species III predominates over those of species I and II. These observations are compatible with H-bond formation between the iron-bound MeO^- and the solvent MeOH. The H-bond formation proceeds in a stepwise fashion,

(24) Collman, J. P.; Gagne, R. R.; Reed, C. A.; Halbert, T. R.; Lang, G.; Robinson, W. T. *J. Am. Chem. Soc.* **1975**, *97*, 1427.
(25) Del Gaudio, J.; La Mar, G. N. *J. Am. Chem. Soc.* **1976**, *98*, 3014. La Mar, G. N.; Del Gaudio, J. *Adv. Chem. Ser.* **1977**, *No. 162*, 207.
(26) Further studies to characterize the electronic and reactive properties of the Fe^{II} species are under way.
(27) Hanson, L. K.; Eaton, W. A.; Sligar, S. G.; Gunsalus, I. C.; Gouterman, M.; Connell, C. R. *J. Am. Chem. Soc.* **1976**, *98*, 2672. White, R. E.; Coon, M. J. *Annu. Rev. Biochem.* **1980**, *49*, 315.
(28) Kim, I. C.; Deal, W. C. *Biochemistry* **1976**, *15*, 4925. Kim, I. C. *J. Biol. Chem.* **1982**, *257*, 1063.
(29) Mincey, T.; Traylor, T. G. *J. Am. Chem. Soc.* **1979**, *101*, 765. Landrum, J. T.; Hatano, K.; Scheidt, W. R.; Reed, C. A. *Ibid.* **1980**, *102*, 6729.
(30) Similar spectra were observed at 15 K and intermediate temperatures, indicating that the three species are not affected by change in temperature below 77 K.

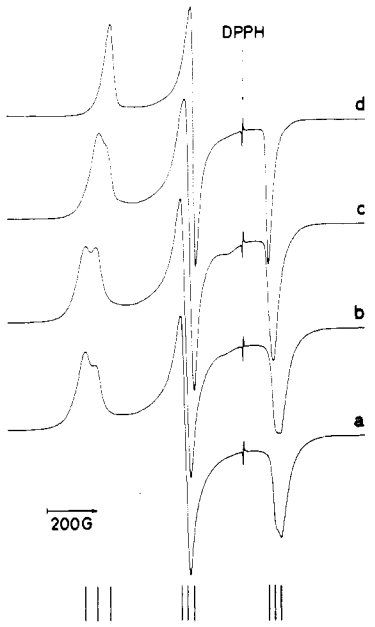

Figure 7. Effect of F^- concentration on EPR spectra of $Fe(TPP)(OMe)_2^-$ at 77 K. Conditions: Me_2SO–MeOH (97:3 v/v); $[Fe(TPP)(Me_2SO)_2^+]_0$ = 1.4 mM; $[MeO^-]_0/[Fe(TPP)(Me_2SO)_2^+]_0$ = 50; $[F^-]_0$ = 0 (a), 100 (b), 200 (c), 500 mM (d). See Figure 5 for peak assignments at the bottom.

species I–III being regarded as starting, intermediate, and ending species, respectively.

(b) MeO^- Concentration. As shown in Figures 2 and 3, the binding of MeO^- to iron takes place stepwise to lead to an increased formation of $Fe(TPP)(OMe)_2^-$ with an increase in MeO^- concentration. On closer examination, however, the low-spin complex $Fe(TPP)(OMe)_2^-$ in Me_2SO–MeOH (99:1 v/v) (Figure 2) is found to vary in its H-bonded state from species III to II to I as MeO^- concentration is increased ($[MeO^-]_0/[Fe(TPP)(Me_2SO)_2^+]_0$ = 2–50, where $[Fe(TPP)(Me_2SO)_2^+]_0$ = 1.4 mM). Species II is observed in preference to species I and III at $[MeO^-]_0/[Fe(TPP)(Me_2SO)_2^+]_0 \simeq 25$. By contrast, the H-bonded state of $Fe(TPP)(OMe)_2^-$ in Me_2SO–MeOH (75:25 v/v) (Figure 3), which corresponds to species III, remains unchanged during the variation of MeO^- concentration ($[MeO^-]_0/Fe(TPP)(Me_2SO)_2^+]_0$ = 2–100). Additional observations proved that MeO^- concentration shows a significant effect on the H-bonded state of $Fe(TPP)(MeO)_2^-$ in the solvent of low MeOH concentration (<5% (v/v)), while it does not in the solvent of relatively high MeOH concentration (>5% (v/v)). The H-bonded state of $Fe(TPP)(OMe)_2^-$ in toluene–MeOH[16] corresponds to species III and was not affected by changes in both MeO^- and MeOH concentrations.

(c) F^- Concentration. Fluoride anion is a powerful H-bond proton acceptor, and a number of strong H bonds of the type XH···F^- (X = F, O, N) are known.[31] The anion F^- would H bond strongly with MeOH when added to Me_2SO–MeOH, thereby decreasing the concentration of MeOH that can H bond to the iron-bound MeO^-. It is expected that addition of F^- brings about a remarkable effect on the H-bonded state of $Fe(TPP)(OMe)_2^-$.

Figure 7 shows the EPR spectral changes that occur when a varying amount of F^- is added to the solution of $Fe(TPP)(OMe)_2^-$ in Me_2SO–MeOH (97:3 v/v). In accord with the above expectation, addition of F^- causes the H-bonded state of $Fe(TPP)(OMe)_2^-$ to greatly change. In the absence of F^-, species II and III, exhibiting comparable spectral intensities, exist in the solution. Upon addition of increasing F^-, the spectrum of species III decreases in its intensity with the concomitant increase in that of species II. The spectrum of species II gains its maximum intensity at the concentration $[F^-]_0 \simeq 200$ mM and is completely replaced by the spectrum of species I at the high concentration $[F^-]_0 \simeq$ 500 mM. The increase in F^- concentration causes species III to convert to species II and I in a stepwise fashion. This effect of F^- concentration presents a striking contrast to that of MeOH concentration. It seems probable that the iron-bound MeO^- competes with F^- for H-bond formation with the solvent MeOH.

Scheme II

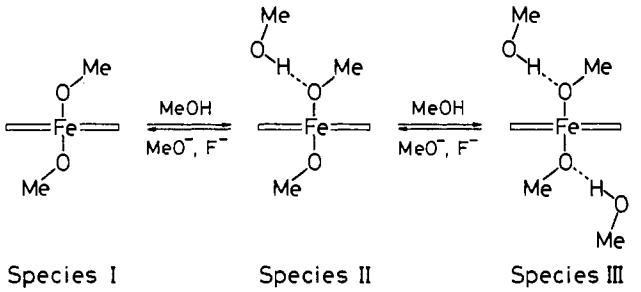

Hydrogen-Bonded States of $Fe(TPP)(OMe)_2^-$. The three spectrally distinct species I–III detected for $Fe(TPP)(OMe)_2^-$ can be characterized in terms of the formation of H bond between the iron-bound MeO^- and the solvent MeOH as depicted in Scheme II. In this scheme it is assumed that the iron-bound MeO^- in species I is not H bonded with MeOH. In view of the fact that species I is observed only at the low MeOH concentration, MeOH is likely associated with unligated MeO^- and solvent Me_2SO as shown in

$$MeOH + MeO^- = MeOH\cdots OMe^- \quad (3)$$

$$MeOH + Me_2SO = MeOH\cdots OSMe_2 \quad (4)$$

Thus, Me_2SO competes with MeO^- for the remaining MeOH and in effect decreases the concentration of MeOH available to the iron-bound MeO^-. Under the condition of low MeOH concentration, MeOH is not capable of forming an H bond with the iron-bound MeO^- (MeO^-–Fe), reaction 5 being difficult to occur.

$$MeOH + MeO^-\text{–}Fe = MeOH\cdots(MeO^-\text{–}Fe) \quad (5)$$

In contrast, as MeOH concentration increases, reaction 5 is expected to proceed, yielding species II and III in a stepwise fashion. It is assumed in Scheme II that only the fifth axial ligand is H bonded with MeOH in species II, while both the fifth and sixth axial ligands are in species III. As described in the preceding section, species III is found in Me_2SO–MeOH of relatively high MeOH concentration (>5% (v/v)). Species III is observed also in pure MeOH, which forms glasses at low temperature. MeOH glasses are considered to consist of long H-bonded chains of branched structure.[32] MeOH molecules with one to three H bonds are found and assigned to species at the ends of chains, in the middle of chains, and at branch points of chains.[32] It appears also likely that the iron-bound MeO^- in species III is linked to a MeOH polymer chain or is H bonded, acting as dibase, with two MeOH molecules. Species II is considered to be intermediate between species I and III in degree of H-bond formation.

The effect of added fluoride anion can be explained reasonably by introducing the H-bond formation equilibrium (6). Thus,

$$MeOH + F^- = MeOH\cdots F^- \quad (6)$$

increasing the F^- concentration lowers the concentration of MeOH capable of forming H bonds with the iron-bound MeO^-, resulting in the stepwise conversion from species III to II to I. Interestingly, F^- is unable to compete with MeO^- for axial coordination sites under the condition studied. It is evident that F^- serves only to remove the H-bonded MeOH from the iron-bound MeO^-, thereby modulating the H-bonded state of $Fe(TPP)(OMe)_2^-$. Such an indirect interaction of F^- with $Fe(TPP)(OMe)_2^-$ shows a marked difference when compared with the interaction of F^- with low-spin complex $Fe(DPIXDME)(ImH)_2^+$,[33] where F^- is considered to H

(31) Emsley, J. *Chem. Soc. Rev.* **1980**, *91*.

(32) Falk, M.; Whalley, E. *J. Chem. Phys.* **1961**, *34*, 1554. Jorgensen, W. L. *J. Am. Chem. Soc.* **1980**, *102*, 543.

(33) Momenteau, M.; Mispelter, J.; Lexa, D. *Biochim. Biophys. Acta* **1973**, *320*, 652.

Table II. Effect of the H Bonding or Deprotonation of Axial Ligands on Crystal Field Parameters of Low-Spin Fe(III) Heme Complexes

low-spin complex/solvent	g_x	g_y	g_z	temp, K	cryst field param δ^b	μ^b	R^c	k	ref
$Fe(TPP)(OMe)_2^-$/Me_2SO-MeOH									
species I	1.942	2.134	2.394	15	10.62	5.30	0.499	1.039	this work
	1.942	2.133	2.395	77	10.71	5.29	0.494	1.039	
species II	1.928	2.151	2.442	15	9.49	4.82	0.508	1.062	this work
	1.929	2.151	2.444	77	9.63	4.85	0.504	1.073	
species III	1.914	2.165	2.494	15	8.85	4.43	0.501	1.096	this work
	1.915	2.164	2.491	77	8.90	4.46	0.501	1.094	
$Fe(TPP)(OMe)_2^-$/toluene-MeOH[a]									
species III	1.914	2.165	2.494	25	8.85	4.43	0.501	1.096	16
	1.915	2.164	2.492	77	8.92	4.45	0.499	1.096	
$Fe(TPP)(ImH)_2^+/CH_2Cl_2$	1.56	2.30	2.92	77	3.35	2.05	0.612	1.055	3
$Fe(TPP)(Im)(ImH)/CH_2Cl_2$	1.74	2.28	2.73	77	4.20	2.73	0.650	1.051	3
$Fe(TPP)(Im)_2^-/CH_2Cl_2$	1.76	2.28	2.73	77	4.47	2.84	0.636	1.083	3

[a] Species I and II could not be detected in toluene-MeOH. [b] In units of ζ (spin-orbit coupling constant, $\zeta \simeq 400$ cm^{-1}). [c] $R = \mu/\delta$.

bond directly with the N-H moiety of coordinated ImH.

The effect of MeO^- concentration can be explained similarly by considering reaction 3 instead of 6. However, in the solvent of high MeOH concentration, the equilibrium (5) lies far to the right and the H-bonded state of species III is affected by addition neither of F^- nor of MeO^-.

In brief, which of species I–III to be formed and stabilized is determined by the H-bond formation equilibria (3)–(6). All the observations are consistent with the assumption that the H-bond formation constant decreases in the order (6) > (3) > (5) > (4). Thus, in the solvent of low MeOH concentration, increasing the MeO^- and/or F^- concentrations leads to the formation of species I in preference to species II and III, while the higher the MeOH concentration in the solvent, the more favorable it is for the formation of species III to take place.

Hydrogen Bonding and Crystal Field Splittings. In general, the modes of H bonding involving the coordinated axial ligands are conveniently divided into two types: M–L–H···X and M–L···H–X, where M–L–H and M–L represent the metal-bound ligand with proton donor and acceptor properties, respectively, and X and X–H, the external proton acceptor and donor, respectively. In the extreme case of proton transfer and H-bond dissociation, the first type, yielding M–L, is regarded as deprotonation, and the second type, yielding M–L–H, as protonation. The two types of H bonding are in a conjugate relation.

The present work on $Fe(TPP)(OMe)_2^-$ demonstrates the second type of H bonding in low-spin Fe(III) heme complexes. The possible protonation as the cause of conversion of species I into II and III is reasonably ruled out, since the high-spin complexes, Fe(TPP)(OMe)(MeOH) and $Fe(TPP)(MeOH)_2^+$,[12] are formed upon protonation of $Fe(TPP)(OMe)_2^-$. The first type of H bonding has been found or suggested in various hemoproteins[5-9] with proximal histidyl imidazole and in some model heme complexes.[2,3,10-12] The simple example that offers a most striking contrast to the present complex $Fe(TPP)(OMe)_2^-$ is the low-spin bis(imidazole) complex $Fe(TPP)(ImH)_2^+$ for which strongly H-bonded or deprotonated forms, Fe(TPP)(Im)(ImH) and $Fe(TPP)(Im)_2^-$, have recently been characterized[3] by EPR spectroscopy. We interpret this example as the extreme case of deprotonation in the first type of H bonding.

The two types of H-bonding interaction are expected to modulate the electronic properties of axial ligands in opposite directions. To demonstrate how the d-orbital energy level is affected by the second type of H bonding, we have analyzed the g values observed for species I–III with the assumption of a pure t_2^5 electron configuration as described previously.[34] The tetragonal and rhombic splittings in the three t_2 orbitals (i.e., d_{yz}, d_{zx}, and d_{xy}), δ and μ, respectively, the crystal field rhombicity R defined as the quantity μ/δ, and the orbital reduction factor k are determined from the three observed values (g_x, g_y, g_z). Such crystal field parameters are given in Table II, where the values are compared with those obtained for the complexes $Fe(TPP)(ImH)_2^+$, Fe(TPP)(Im)(ImH), and $Fe(TPP)(Im)_2^-$ with progressively increased degree of deprotonation.

It is seen that the crystal field rhombicity R and the orbital reduction factor k remain almost constant among the three species $Fe(TPP)(OMe)_2^-$. The k values fall within the range from 1.0 to 1.1, indicating that the three low-spin species belong to the normal class of low-spin Fe(III) heme complexes. The rhombicity R is related to the geometrical arrangement of the iron ligands and to the π bonds between these ligands and the iron atom[35] and, as such, is a good measure of the intrinsic asymmetry in low-spin heme complexes where the axial ligands are chemically equivalent and approximately parallel.[36] Thus, the calculated R values, which fall within a narrow range from 0.49 to 0.51, are taken to indicate that species I–III have similar geometrical arrangement of the axial MeO^- ligands. It appears well established that the H-bond formation does not alter the geometry of the nearest coordination sphere of $Fe(TPP)(OMe)_2^-$. The same can be said of the low-spin complexes $Fe(TPP)(ImH)_2^+$, Fe(TPP)(Im)(ImH), and $Fe(TPP)(Im)_2^-$.

In contrast, it is found that the tetragonal and rhombic splittings, δ and μ, respectively, decrease significantly on going from species I to II to III, while they increase by almost the same amount from $Fe(TPP)(ImH)_2^+$ to Fe(TPP)(Im)(ImH) to $Fe(TPP)(Im)_2^-$. These opposite trends in δ and μ, as the H-bonding interaction increases, are quite reasonable, since the axial ligand acts as an H-bond acceptor in $Fe(TPP)(OMe)_2^-$, while it does as a proton donor in $Fe(TPP)(ImH)_2^+$. The value δ is primarily dependent upon the charge on the iron atom,[35] which is a function of the electron donation by the two axial ligands. The observed trends in δ and μ are, therefore, consistent with the view that the second type of H bonding reduces the π donor strength of axial ligands, while the first type enhances their π donor strength. It must be conceded that the σ donor strength is affected similarly by changes in H-bonding interaction. The H bonding of axial ligands seems to be in control of the electron density at the iron by means of the synergism between π- and σ-bonding effects.

On the basis of these considerations, it becomes evident that an increase in degree of the H-bond formation in $Fe(TPP)(OMe)_2^-$ results in leess negative charge donated to the iron from the coordinated MeO^-. Such an electronic situation may be effected in species III, offering a probable explanation for the observation that species III is relatively stable toward the autoreduction. By contrast, in the absence of H bonding as in species I, the coordinated MeO^- acts as a stronger field ligand, causing the electron

(34) Sato, M.; Ohya, T.; Morishima, I. *Mol. Phys.* **1981**, *42*, 475.

(35) Blumberg, W. E.; Peisach, J. In "Probes of Structure and Function of Macromolecules and Membranes"; Chance, B., Yonetani, T., Mildvan, A. S., Eds.; Academic Press: New York, 1971; Vol. 2, p 215. Chevion, M.; Peisach, J.; Blumberg, W. E. *J. Biol. Chem.* **1977**, *252*, 3637. Hollenberg, P. F.; Hager, L. P.; Blumberg, W. E.; Peisach, J. *Ibid.* **1980**, *255*, 4801.

(36) Byrn, M. P.; Katz, B. A.; Keder, N. L.; Levan, K. R.; Magurany, C. J.; Miller, K. M.; Pritt, J. W.; Strouse, C. E. *J. Am. Chem. Soc.* **1983**, *105*, 4916.

density at the iron to increase. This opposite electronic situation makes species I unstable toward the autoreduction. The solvent-dependent autoreduction found for $Fe(TPP)(OMe)_2^-$ in Me_2SO–MeOH is interpreted in terms of such H-bonding effects. This interpretation is in keeping with the findings by Del Gaudio et al.[37] that the autoreduction of $Fe(TPP)(Pip)_2^+$ is facilitated by the deprotonation of the coordinated piperidine.

In sum, it has been amply demonstrated that the d-orbital energy level of the low-spin complex $Fe(TPP)(OMe)_2^-$ is modulated by the H-bond formation between the iron-bound MeO^- and the solvent MeOH. The H bonding weakens the axial ligand field, thereby causing alterations in electron density and reactivity at the central metal ion. The present model system is a simple example showing that heme reactivity is controlled by H bonding and as such, would help our understanding of electronic control of heme reactivity in various hemoproteins.

Acknowledgment. This work was supported in part by grants from the Ministry of Education, Japan. The authors are grateful to Dr. H. Kon for continuous encouragement.

Registry No. $Fe(TPP)(OMe)_2^-$, 89709-81-9.

(37) Del Gaudio, J.; La Mar, G. N. *J. Am. Chem. Soc.* **1978**, *100*, 1112.

Contribution from the Department of Chemistry, University of Florence, Florence, Italy

Homo- and Heterodimer Formation in Metalloporphyrins

LUCIA BANCI

Received April 26, 1984

The dimer formation constants in chloroform for CuP, AgP, and VOP, where P is mesoporphyrin IX dimethyl ester, have been obtained through EPR measurements at room temperature and spectral simulation. For CuP, measurements have been performed also in 1,1,2,2-tetrachloroethane and dichloromethane, and aggregation was found to be sensibly different in the three solvents. Heterodimer formation constants have been determined between the above metalloporphyrins and FePCl. Invariably the latter constants are larger than expected on the basis of the homodimer formation constants. The frozen-solution EPR spectra of CuP and AgP have provided the spectra of the pure dimeric species through computer manipulation. Evidence of two dimeric species is provided by the frozen-solution EPR spectra of VOP.

Introduction

It is well-known that porphyrins and metalloporphyrins tend to aggregate in solution. Several constants relative to dimer formation are available on porphyrins and metalloporphyrins in water solution and in organic solvents;[1,2] however, the factors determining the extent of dimer formation like the nature of the metal ion, the solvent, the planar or square-pyramidal geometry around the metal ion, and the kind of homo- or heterometallodimer are not yet fully understood. Owing to the relevance of this class of compounds as such and as models of naturally occurring metalloporphyrins, we thought it interesting to further investigate the tendency to aggregate of several metal derivatives of the mesoporphyrin IX dimethyl ester (MP hereafter) around room temperature in several solvents and to analyze the EPR spectra of the dimers at liquid-nitrogen temperature.

We have devised a procedure to determine the affinity constants for self-aggregation through EPR spectroscopy for those metal complexes that display EPR signals at room temperature such as the complexes of Cu^{2+}, Ag^{2+}, and VO^{2+}. Aggregation of such metalloporphyrins causes a decrease of the electronic relaxation times, and the EPR spectra at room temperature become very broad, possibly beyond detection. Therefore, the decrease in signal intensity of the monomeric species upon increase of solute concentration is related to solute aggregation. This holds also when a Cu^{2+}, Ag^{2+}, or VO^{2+} porphyrin interacts with a metalloporphyrin like mesoporphyrin IX dimethyl ester iron(III) chloride (FePCl), which does not show detectable EPR signal at room temperature. The latter derivative is five-coordinated with a chloride in the apical position of a square pyramid.[3]

Experimental Section

Metal-free mesoporphyrin IX dimethyl ester was provided by Sigma Chemical Co. and used without further purification. Its Cu(II), Ag(II), and Fe(III) complexes were prepared from the halides (Cu, Fe) or acetate (Ag) salts in dimethylformamide,[4] whereas the VO^{2+} derivative was prepared from the acetylacetonate in phenol.[5] They were purified by thin-layer chromatography on silica gel using a mixture CH_2Cl_2/CH_3CN (98:2). The electronic absorption maxima and the EPR spectra of CuP and AgP are the same as those reported in the literature.[6-8] The absorption maxima and the molar absorbance of VOP and FePCl solutions fully agree with literature data.[9,10]

All the solvents were of analytical grade and were used without further purification.

The EPR spectra were recorded at X-band frequency with 100-kHz modulation on a Bruker ER200 spectrometer interfaced with the computer Aspect 2000 and equipped with a variable-temperature controller. The spectra of the solutions were recorded at 25 °C; particular care was taken to obtain highly reproducible spectra and intensities. Each spectrum was simulated in order to appreciate the line width. The spectra at liquid-nitrogen temperature of concentrated solutions have been recorded as glasses in 1,1,2,2-tetrachloroethane. The spectra of the monomeric species obtained on glasses of dilute solutions, when possible, were subtracted, after appropriate scaling, from those of the concentrated glasses, in such a way to have cleaner spectra of the dimeric species.

Results

Determination of Affinity Constants. For Homodimers CuP–CuP, AgP–AgP, and VOP–VOP. The EPR spectra were recorded at different concentrations of metalloporphyrin from 1×10^{-4} M to saturation ($\sim(2-6) \times 10^{-2}$ M). By taking into account the different gain when the spectra were recorded and by correcting for different concentrations, the same signal intensity would be expected for all the samples as if there were no concentration-dependent equilibria. Actually a sizable decrease in corrected intensity with increasing concentration is observed. Instead of the actual intensity measured through double integration of the signal, we have taken into consideration the height of either the hyperfine or superhyperfine splitted lines. Such heights should

(1) White, W. I. In "The Porphyrins"; Dolphin, D., Ed.; Academic Press: New York, 1978; Vol. V, p 303.
(2) Scheer, H.; Katz, J. J. In "Poprhyrins and Metalloporphyrins"; Smith, K. M., Ed.; Elsevier: Amsterdam, 1975; Chapter 10.
(3) Hoord, J. L.; Cohen, G. H.; Glick, M. D. *J. Am. Chem. Soc.* **1967**, *89*, 1992.
(4) Adler, A. D.; Longo, F. R.; Kampas, F.; Kim, J. *J. Inorg. Nucl. Chem.* **1970**, *32*, 2443.
(5) Buchler, J. W.; Eikelmann, G.; Puppe, L.; Rohbock, K.; Schneehage, H. H.; Weck, D. D. *Justus Liebigs Ann. Chem.* **1971**, *745*, 135.
(6) Konishi, S.; Hoshino, M.; Imamura, M. *J. Phys. Chem.* **1982**, *86*, 4888.
(7) Yokoi, H.; Iwaizumi, M. *Bull. Chem. Soc. Jpn.* **1980**, *53*, 1489.
(8) MacCragh, A.; Storm, C. B.; Koski, W. S. *J. Am. Chem. Soc.* **1965**, *87*, 1470.
(9) Erdman, J. G.; Corwin, A. H. *J. Am. Chem. Soc.* **1947**, *69*, 751.
(10) Erdman, J. G.; Ramsey, V. G.; Kalenda, N. W.; Hanson, W. E. *J. Am. Chem. Soc.* **1956**, *78*, 5844.

0020-1669/85/1324-0782$01.50/0